Nonlinear Symmetric Instability and Intraseasonal Oscillations in the Tropical Atmosphere

J.-X. ZHAO AND M. GHIL

Climate Dynamics Center, Department of Atmospheric Sciences and Institute of Geophysics and Planetary Physics, University of California, Los Angeles, California

(Manuscript received 18 June 1990, in final form 24 March 1991)

ABSTRACT

Symmetric inertial instability (SII) is studied here as a mechanism for stratospheric and tropospheric phenomena in the equatorial regions. We investigate the linear and nonlinear dynamics of SII in a two-layer, zonally symmetric model on an equatorial beta plane, in the presence of a basic flow with horizontal and vertical shear, with and without dissipative effects.

Linear symmetric instabilities are, in accordance with previously published results, purely exponential, that is, nonoscillatory. Nonlinear SII, studied here for the first time on a planetary scale, can produce finite-amplitude oscillatory behavior, periodic or chaotic. The period of oscillations in the inviscid case depends on the initial data. In the presence of dissipative effects, all solutions tend to a limit cycle or to a strange attractor. The dominant period in this case, over a wide range of parameters and whether vertical shear is present or not, is in the intraseasonal, 20–30-day range. It appears therefore that nonlinear SII might be a contributing mechanism to low-frequency oscillations in the tropical atmosphere.

1. Introduction

The dynamical origin of atmospheric disturbances is commonly sought in linear instabilities with spatial and temporal properties reminiscent of the observed disturbances. The theory of symmetric inertial instability (hereafter SII), or symmetric overturning, is one of the classic hydrodynamical problems, having found significant applications in meteorology. The general nature of and criterion for this instability were first discussed by Helmholtz (1888) and Rayleigh (1916). An explicit instability criterion was given by Solberg (1936), and an integral derivation by Fjørtoft (1944, 1950). Ooyama (1966) gave a rigorous demonstration of a sufficient criterion for instability through an initial-value approach, while Yanai and Tokioka (1969) carried out detailed numerical experiments on SII.

Several applications of SII to atmospheric motion have been proposed. Emanuel (1979, 1983), Xu (1986, 1988, 1989), and Thorpe and Rotunno (1989) discussed linear and nonlinear SII in relation to mesoscale disturbances and rainbands. Dunkerton (1981) suggested that it plays an important role in the tropical middle atmosphere. SII was also recognized by Hunt (1981) in his numerical work on the maintenance of the zonal circulation in the middle atmosphere. Asymmetric inertial instability was analyzed by Boyd and Christidis (1982) and by Dunkerton (1983).

Corresponding author address: Michael Ghil, University of California, Los Angeles, 405 Hilgard Avenue, Los Angeles, CA 90024.

Stevens (1983) extended the idea of SII into the equatorial troposphere in order to explore the possibility that a source of energy for the 40–50-day tropical oscillation may lie in nonvanishing meridional shear of the zonal flow. Anderson and Rosen (1983) and Krishnamurti and colleagues (1982, 1988) also suggested that 40–50-day oscillations in the equatorial zonal mean wind (Madden and Julian 1971), as well as in certain zonally asymmetric fields such as the monsoon circulation, could result from SII.

A number of difficulties arise in trying to apply the inertial instability concept to oscillating phenomena over the tropics. First, as pointed out by Dunkerton (1981), SII prefers the smallest vertical scales, so that diffusion processes must be involved in applications to the mesosphere. The vertical scale in the troposphere is hard to determine unequivocally. Linear eigenanalysis gives very different equivalent depths, depending on whether moist effects are included or not (Anderson and Stevens 1987). Second, linear SII theory (Dunkerton 1981; Stevens 1983) gives only nonoscillating, purely exponential growth, which is hard to associate with oscillating phenomena. The asymmetric instability discussed by Dunkerton (1983) gives Kelvin-like unstable waves.

The purpose of this paper is to exhibit an oscillating symmetric instability, which might be related more easily to oscillatory phenomena in the equatorial troposphere. It turns out that such an instability does arise in a two-layer, nonlinear symmetric model, which is a crude approximation for tropospheric flow. The key

question concerns the dynamics of the oscillating mechanism for the inevitable SII due to horizontal shear at the equator.

The equatorial β-plane model is described in section 2. In section 3, following Dunkerton (1981), Boyd and Christidis (1982), and Stevens (1983), a basic flow with superposed linear and parabolic horizontal profiles is considered in order to study linear SII. The vertical shear of the basic flow, which results in nonseparation of vertical and meridional modes (Boyd 1978a,b), is neglected in this section. A weakly nonlinear theory is developed in section 4, and the oscillating behavior of nonlinear SII is presented in section 5. The effects of weak vertical shear on this nonlinear SII are investigated in section 6. Concluding remarks follow in section 7.

2. Model description

The vertical structure of the equatorial troposphere is quite complicated. But the basic dynamic feature of its zonal mean flow is the reversal between the upper and the lower level, indicating the dominance of the first baroclinic mode. Higher-order vertical modes in the troposphere are much weaker. For the study of inertial instability, we assume therefore that the tropical troposphere is well mixed due to convective processes (Stevens and Lindzen 1978), so that the higher vertical modes are strongly suppressed. Based on this assumption, we can prefilter the governing equations by choosing a simple two-layer approximation.

In such a model we only consider Rayleigh-type friction, which is independent of vertical scale, and a simple basic flow $(\bar{u}_i, 0, 0)$, $i = 1, 3$. The horizontal wind profile for the latter is taken as the sum of linear and quadratic terms. The vertical shear is only represented by use of different constants in this profile at the upper and the lower level. Thus, we assume

$$\bar{u}_i = U_i + \gamma y + \frac{\delta}{2} y^2, \quad i = 1, 3. \quad (2.1a,b)$$

In the two-layer model, variables are assigned to the two main levels, labeled $i = 1, 3$, and to the auxiliary levels $i = 0, 2, 4$, as shown in Fig. 1. In this model, the zonally symmetric equations in pressure coordinates on an equatorial β plane are

$$\frac{\partial u_1}{\partial t} + v_1 \frac{\partial u_1}{\partial y} + \frac{\omega_2}{2\Delta p}(u_3 - u_1) - \left(\beta y - \frac{\partial \bar{u}}{\partial y}\right) v_1 = -r u_1, \quad (2.2a)$$

$$\frac{\partial u_3}{\partial t} + v_3 \frac{\partial u_3}{\partial y} + \frac{\omega_2}{2\Delta p}(u_3 - u_1) - \left(\beta y - \frac{\partial \bar{u}}{\partial y}\right) v_3 = -r u_3, \quad (2.2b)$$

$$\frac{\partial v_1}{\partial t} + v_1 \frac{\partial v_1}{\partial y} + \frac{\omega_2}{2\Delta p}(v_3 - v_1) - \beta y u_1 = -\frac{\partial \phi_1}{\partial y} - r v_1, \quad (2.2c)$$

$$\frac{\partial v_3}{\partial t} + v_3 \frac{\partial v_3}{\partial y} + \frac{\omega_2}{2\Delta p}(v_3 - v_1) - \beta y u_3 = -\frac{\partial \phi_3}{\partial y} - r u_3, \quad (2.2d)$$

$$\frac{\partial v_1}{\partial y} + \frac{\omega_2}{2\Delta p} = 0, \quad (2.2e)$$

$$\frac{\partial v_3}{\partial y} - \frac{\omega_2}{2\Delta p} = 0, \quad (2.2f)$$

$$\frac{\partial(\phi_1 - \phi_3)}{\partial t} - \Delta p S \omega_2 = -\mu(\phi_1 - \phi_3) + Q_2 - v_2 \frac{\partial(\phi_1 - \phi_3)}{\partial y}. \quad (2.2g)$$

The Coriolis parameter f is replaced by βy, Δp is the constant pressure difference between the two layers, $\Delta p = 500$ mb, S is the static stability factor, and Q_2 is the forcing due to diabatic heating, while r and μ are friction and Newtonian-cooling coefficients, respectively. We assume $r = \mu$ hereafter.

It is convenient to introduce the notation

$$f_m = \frac{f_1 + f_3}{2}, \quad f_s = \frac{f_1 - f_3}{2}, \quad (2.3a,b)$$

for the vertical-mean component f_m and the vertical-shear component f_s of each variable $f_i = u_i, v_i, \phi_i$. From the continuity equations (2.2e, f), it follows that

$$\frac{\partial v_m}{\partial y} = 0. \quad (2.4)$$

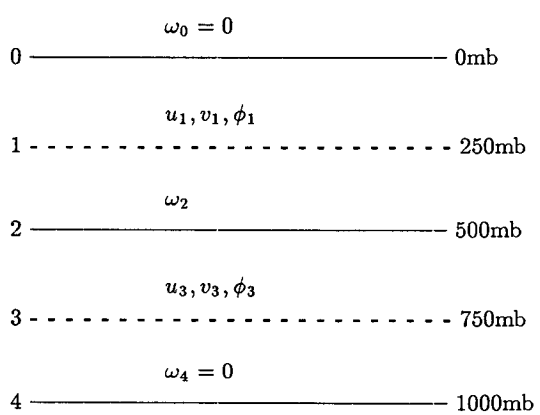

FIG. 1. Vertical structure of the two-level model: u, v, and ω are eastward, northward, and upward velocity, and ϕ is geopotential height.

Hence one can take $v_m \equiv 0$, without loss of generality, and the system (2.2) can be reduced to

$$\frac{\partial u_m}{\partial t} + ru_m + \frac{\partial (v_s u_s)}{\partial y} + \bar{u}_s \frac{\partial v_s}{\partial y} = 0, \quad (2.5a)$$

$$\frac{\partial (v_s v_s)}{\partial y} + \beta y u_m = -\frac{\partial \phi_m}{\partial y}, \quad (2.5b)$$

$$\frac{\partial u_s}{\partial t} + ru_s + v_s \frac{\partial u_m}{\partial y} - \left(\beta y - \frac{\partial \bar{u}}{\partial y}\right) v_s = 0, \quad (2.5c)$$

$$\frac{\partial v_s}{\partial t} + rv_s + \beta y u_s = -\frac{\partial \phi_s}{\partial y}, \quad (2.5d)$$

$$\frac{\partial \phi_s}{\partial t} + c^2 \frac{\partial v_s}{\partial y} = -r\phi_s + \frac{Q_2}{2}. \quad (2.5e)$$

Here $\bar{u}_s = (U_1 - U_3)/2$ is the vertical shear of the basic flow and $c^2 = (\Delta p)^2 S/2$ is the reduced phase speed of gravity waves. We include moist processes into the model implicitly by taking S as the moist static stability. Therefore, we chose a small value of 30 m s^{-1} for c, as listed in Table 1.

Nondimensional quantities are defined by

$$(u_m, u_s, v_s) = U(u'_m, u'_s, v'_s), \quad (2.6a)$$

$$(\phi_m, \phi_s) = cU(\phi'_m, \phi'_s), \quad (2.6b)$$

$$y = ly', \quad t = \tau t', \quad \tau = l/c, \quad \beta_a = \beta - \delta, \quad (2.6c)$$

$$l^2 = \frac{c}{\sqrt{\beta \beta_a}}, \quad \nu = \frac{U}{c}, \quad r = \tau^{-1} r', \quad \frac{Q_2}{2} = \frac{cU}{\tau} Q', \quad (2.6d)$$

$$\xi_0 = \frac{\gamma}{2l\beta_a}, \quad \zeta = \tau \bar{u}_s; \quad (2.6e)$$

here l is the internal Rossby radius of deformation for the β plane, δ is defined in Eq. (2.1), and τ is the time scale of internal gravity waves. The nondimensional form of (2.5), dropping primes, is

TABLE 1. Basic model parameters and nondimensional numbers.

β	Equatorial β parameter	2.3×10^{-11} m^{-1} s^{-1}
Δp	Pressure depth of the half atmosphere	500 mb
c	Gravity-wave phase speed	30 m s^{-1}
r	Friction or Newtonian cooling coefficient	0.3×10^{-5} s^{-1}
γ	Linear shear of basic flow	1.0×10^{-5} s^{-1}
δ	Curvature of basic flow profile	2.1×10^{-11} m^{-1} s^{-1}
$\beta_a = \beta - \delta$		0.2×10^{-11} m^{-1} s^{-1}
l	Horizontal scale	2.0×10^6 m
$\tau = l/c$	Time scale of gravity wave	$\frac{2}{3}$ day
$\epsilon^{1/2}$	The order of supercritical wind shear	0.4 ~ 0.5

$$\frac{\partial u_m}{\partial t} + \nu \frac{\partial (v_s u_s)}{\partial y} + ru_m + \zeta \frac{\partial v_s}{\partial y} = 0, \quad (2.7a)$$

$$\nu \frac{\partial (v_s v_s)}{\partial y} + \left(\frac{\beta}{\beta_a}\right)^{1/2} y u_m = -\frac{\partial \phi_m}{\partial y}, \quad (2.7b)$$

$$\frac{\partial u_s}{\partial t} + \nu v_s \frac{\partial u_m}{\partial y} - \left(\frac{\beta_a}{\beta}\right)^{1/2} (y - 2\xi_0) v_s = -ru_s, \quad (2.7c)$$

$$\frac{\partial v_s}{\partial t} + \left(\frac{\beta}{\beta_a}\right)^{1/2} y u_s = -\frac{\partial \phi_s}{\partial y} - rv_s, \quad (2.7d)$$

$$\frac{\partial \phi_s}{\partial t} + \frac{\partial v_s}{\partial y} = -r\phi_s + Q. \quad (2.7e)$$

The first-order differential equations (2.7d–e) yield, by elimination, the second-order equation:

$$\frac{\partial^2 v_s}{\partial y^2} - \frac{\partial^2 v_s}{\partial t^2} - y(y - 2\xi_0) v_s = \frac{\partial Q}{\partial y} - \left(\frac{\beta}{\beta_a}\right)^{1/2} \nu y v_s \frac{\partial u_m}{\partial y} + 2r \frac{\partial v_s}{\partial t} + r^2 v_s \quad (2.8)$$

for v_s. Equation (2.8), combined with (2.7a,c), is equivalent to system (2.7), subject to suitable boundary conditions. The two systems (2.7a–e) and (2.7a,c; 2.8) will be used alternatively throughout the rest of this paper.

3. Linear analysis

Neglecting nonlinear terms and the vertical shear of the basic flow, as well as dissipation and heating—

$$\zeta = 0, \quad r = 0, \quad Q = 0, \quad (3.1)$$

we consider a linear, inviscid, and unforced version of our problem. Equation (2.8) becomes therewith

$$Lv_s \equiv \left\{\frac{\partial^2}{\partial y^2} - \frac{\partial^2}{\partial t^2} - y(y - 2\xi_0)\right\} v_s = 0. \quad (3.2)$$

Assuming

$$v_s = V(y) e^{i\sigma t} \quad (3.3)$$

yields a classical eigenvalue problem,

$$\frac{\partial^2 V}{\partial \eta^2} + (\sigma^2 + \xi_0{}^2 - \eta^2) V = 0, \quad (3.4a)$$

$$|V_\eta| < \infty, \quad \eta \equiv y - y_0 \to \pm\infty, \quad (3.4b,c)$$

where $y_0 = \xi_0$. The eigenvalues and eigenfunctions of problem (3.4) are:

$$\sigma^2 + \xi_0{}^2 = 2n + 1, \quad n = 0, 1, 2, 3, \cdots, \quad (3.5a)$$

$$V_n = V(t) D_n(\sqrt{2}\eta), \quad (3.5b)$$

where D_n is the nth-order parabolic cylinder function.

If the constant component of the horizontal shear of the basic flow vanishes, $\gamma = 0$, then $\xi_0 = 0$, and we

get neutral symmetric oscillations of gravity-wave type with frequency:

$$\sigma = \pm\sqrt{2n+1}, \quad n = 0, 1, 2, 3, \cdots. \quad (3.6)$$

It is clear from Table 1, for the parameters chosen, that the linear time scale is around a day or so. Therefore, these neutral oscillations are high-frequency standing waves with a period of a few hours.

However, for $\gamma \neq 0$ and hence $\xi_0 \neq 0$, we find that

$$|\xi_0| > \xi_c(n) \equiv \sqrt{2n+1} \quad (3.7)$$

yields exponentially growing modes. This is the symmetric inertial instability (SII) discussed for tropical motions by Dunkerton (1981, 1982). From Eq. (2.5), it can be easily shown that the energy source that fuels the instability is the conversion of the basic flow's kinetic energy to perturbation energy through downgradient momentum transport. From (3.7), it follows that the most unstable mode, the one with $n = 0$, requires only that $|\xi_0| > 1$.

From (2.6e), we find that ξ_0 depends on both γ and δ in the basic wind profile (2.1). The larger the constant shear coefficient γ along the equator, the more unstable the basic flow is. Small β_a also favors the instability. This means [cf. (2.6c)] that, if the barotropically stabilizing effect of β is reduced substantially by the curvature δ of the wind profile, a critical value of γ is more easily achieved for SII to occur. It is clear from the definition of ξ_0 that a smaller reduced-gravity wave speed favors the achievement of ξ_{0c}.

In general, the instability criterion (3.7) is hard to satisfy for a dry atmosphere and linear shear of the basic flow. For a realistic shear γ on the order of 10^{-5} s^{-1} and S reduced by moist processes, yielding c as in Table 1, a relatively larger curvature of basic flow δ is required to make the basic flow unstable, $\beta_a \approx \beta/10 \ll \beta$. In other words, when the stabilization effect of β is nearly canceled by the basic-flow vorticity gradient, SII for the gravest vertical mode is possible. This is the case in the tropics, where the planetary vorticity gradient is quite small.

For the plausible parameter values in Table 1, we find that ξ_0 can exceed $\xi_c(0)$, so an inertial instability does occur. For the unstable modes, however, the frequency is identically zero and the amplitude increases exponentially in time, without oscillating.

Stevens (1983) suggested that the existence of zonally symmetric and asymmetric inertial instabilities in the tropics provides a possible mechanism for exciting the 40–50-day oscillation in the equatorial troposphere. However, linear symmetric inertial instabilities, in a dry atmosphere, are nonoscillatory. Stevens also pointed out that moist processes might yield a complex c^2 and lead therewith to an oscillatory instability. This is a definite possibility, which we do not mean to exclude, although we are including the effect of moist processes merely to reduce static stability.

On the other hand, Pedlosky (1971, 1972) showed that a balance between nonlinear saturation and linear growth can also lead to finite-amplitude oscillatory behavior in a baroclinic atmosphere, in the presence of additional instabilities. This is a common feature in fluid dynamics. In the next three sections, we explore various finite-amplitude oscillations produced by nonlinearity in our simple symmetric system. It turns out that the saturation of exponential growth for the linear symmetric instability leads to a more complicated steady flow, which is subject to an oscillatory instability. It is the saturation of the latter that leads to the finite-amplitude low-frequency oscillations of interest here.

4. Weakly nonlinear analysis

The linear analysis of the preceding section shows that horizontally sheared basic flow on an equatorial β plane is subject to inertial instability when the absolute value of the nondimensional parameter ξ_0 exceeds a critical value. The lowest critical value of the horizontal shear parameter $|\xi_0|$ is

$$\xi_{0c} \equiv \xi_c(0) = 1. \quad (4.1)$$

We consider in this section a basic flow which is weakly unstable, that is,

$$\xi_0 = \xi_{0c} + \frac{\Delta\xi}{2}, \quad (4.2a)$$

with $|\Delta\xi/\xi_{0c}| \ll 1$, so that the growth rate is also small. Negative values,

$$\xi_0 = -\xi_{0c} - \frac{\Delta\xi}{2}, \quad (4.2b)$$

are treated in an entirely analogous manner. Equations (4.2) and (3.5) yield

$$\sigma = O(\Delta\xi). \quad (4.3)$$

This gives a slow time scale for the amplitude development of the unstable mode [cf. (3.3)]. Because the growth is slow, it is possible for weak nonlinearity to counterbalance it and to obtain finite-amplitude solutions by the multiple-scale method.

A key ingredient for the successful application of this method is the correct ordering of the different terms in the equations. This ordering is suggested by dynamical considerations arising from the physics of the problem. In the tropics, mean meridional circulation is quite weak compared with the zonal flow; that is, v_s is much smaller in magnitude than u_s and ϕ_s. Meanwhile, when there is no barotropic forcing and vertical mean shear, nonlinear energy conversion from the baroclinic mode to the barotropic mode is the only possible source for the excitation of the latter in the present model. Nonlinear advection is not the dominant process in the momentum and heat budgets, which means that the assumption of weak nonlinearity can give a satisfactory solution. Weak nonlinearity im-

plies in turn that the barotropic mode is much weaker than the baroclinic one.

It is clear from these considerations that the meridional and zonal momentum equations have balances of different orders in the problem's parameters. By carefully matching these balances, we have the following expansions:

$$\xi_0 = \xi_{0c} + \epsilon\xi_0^{(1)}, \quad v_s = \epsilon(v_s^{(1)} + \epsilon v_s^{(2)} + \cdots), \tag{4.4a,b}$$

$$u_s = \epsilon^{1/2}(u_s^{(1)} + \epsilon u_s^{(2)} + \cdots), \quad \phi_s = \epsilon^{1/2}(\phi_s^{(1)} + \epsilon\phi_s^{(2)} + \cdots), \tag{4.4c,d}$$

$$\phi_m = \epsilon(\phi_m^{(1)} + \epsilon\phi_m^{(2)} + \cdots), \quad u_m = \epsilon(u_m^{(1)} + \epsilon u_m^{(2)} + \cdots), \tag{4.4e,f}$$

$$t = \epsilon^{-1/2}T, \quad r = \epsilon^{-1/2}R, \quad Q = 0, \tag{4.4g,h,i}$$

where ϵ is the size of the linear instability exponent. These expansions support the physical intuition that the leading-order balance is geostrophic, between u_s and ϕ_s, and that the barotropic mode is small compared to the baroclinic mode. Recalling that the basic time scale is of one day, the weak friction assumption in (4.4h) will be valid for a reasonable choice of damping time scale, up to three days.

For simplicity, we neglect at first the vertical shear of the basic flow. Equation (2.7) can be rewritten as

$$\frac{\partial u_m}{\partial t} + \nu\frac{\partial(v_s v_s)}{\partial y} + ru_m = 0, \tag{4.5a}$$

$$\nu\frac{\partial(v_s v_s)}{\partial y} + \left(\frac{\beta}{\beta_a}\right)^{1/2} yu_m = -\frac{\partial\phi_m}{\partial y}, \tag{4.5b}$$

$$\frac{\partial u_s}{\partial t} + \nu v_s\frac{\partial u_m}{\partial y} - \left(\frac{\beta_a}{\beta}\right)^{1/2}(y - 2\xi_0)v_s = -ru_s, \tag{4.5c}$$

$$\frac{\partial v_s}{\partial t} + \left(\frac{\beta}{\beta_a}\right)^{1/2} yu_s = -\frac{\partial\phi_s}{\partial y} - rv_s, \tag{4.5d}$$

$$\frac{\partial\phi_s}{\partial t} + \frac{\partial v_s}{\partial y} = -r\phi_s. \tag{4.5e}$$

Substituting (4.4) into (4.5) yields the equations for first-order balance, O(ϵ):

$$\frac{\partial u_s^{(1)}}{\partial T} - \left(\frac{\beta_a}{\beta}\right)^{1/2}(y - 2\xi_0)v_s^{(1)} = -Ru_s^{(1)}, \tag{4.6a}$$

$$\left(\frac{\beta}{\beta_a}\right)^{1/2} yu_s^{(1)} = -\frac{\partial\phi_s^{(1)}}{\partial y}, \tag{4.6b}$$

$$\frac{\partial\phi_s^{(1)}}{\partial T} + \frac{\partial v_s^{(1)}}{\partial y} = -R\phi_s^{(1)}, \tag{4.6c}$$

$$\frac{\partial u_m^{(1)}}{\partial T} + \nu\frac{\partial v_s^{(1)}u_s^{(1)}}{\partial y} = Ru_m^{(1)}. \tag{4.6d}$$

From (4.5), or using (2.8) and (4.4), we have

$$\frac{\partial^2 v_s^{(1)}}{\partial\eta^2} + (\xi_{0c}^2 - \eta^2)v_s^{(1)} = 0, \tag{4.7}$$

where η is defined in (3.4). Recalling that $\xi_{0c} = 1$, the solution for $v_s^{(1)}$ is, separating variables,

$$v_s^{(1)} = V_s(T)H_{vs}(y), \tag{4.8a}$$

$$H_{vs}(y) = D_0(\sqrt{2}\eta). \tag{4.8b}$$

Here $V_s(T)$ is the amplitude of the meridional velocity, yet to be determined, while $H_{vs}(y)$ is its meridional profile. Similarly, let

$$u_s^{(1)} = U_s(T)H_{us}(y), \tag{4.9a}$$

$$\phi_s^{(1)} = \Phi_s(T)H_{\phi s}(y), \tag{4.9b}$$

and, without loss of generality, we get

$$\frac{\partial U_s}{\partial T} + RU_s = V_s, \tag{4.10}$$

which means that the zonal flow acceleration is due to the imbalance between Coriolis force of the meridional circulation and friction force.

The horizontal structure functions H_{us} and $H_{\phi s}$ are determined by the eigenfunctions of the linear analysis:

$$H_{us} = a_0 D_0(\sqrt{2}\eta) + a_1 D_1(\sqrt{2}\eta), \tag{4.11a}$$

$$H_{\phi s} = \frac{\sqrt{2}}{2} D_1(\sqrt{2}\eta), \tag{4.11b}$$

$$a_0 = -\xi_{0c}\left(\frac{\beta_a}{\beta}\right)^{1/2}, \quad a_1 = \frac{\sqrt{\beta_a/\beta}}{\sqrt{2}}. \tag{4.11c,d}$$

The solutions for u_m and ϕ_m can also be obtained by separating variables:

$$u_m^{(1)} = U_m(T)H_{um}(y), \tag{4.12a}$$

$$\phi_m^{(1)} = \Phi_m(T)H_{\phi m}(y). \tag{4.12b}$$

They are given by

$$H_{um} = -\frac{\partial}{\partial y}(H_{vs}(y)H_{us}(y)), \tag{4.13a}$$

$$\frac{\partial U_m}{\partial T} = \nu U_s V_s - RU_m. \tag{4.13b}$$

Equations (4.13a,b) show that the weak barotropic mode is produced by the nonlinearity in momentum advection of the baroclinic mode.

The meridional profiles of the shear components u_s, v_s, and ϕ_s, to first order, are shown in Fig. 2. It is clear that, for the first mode, meridional velocity (dotted) does not change sign, except that it is just opposite in the upper than in the lower level; this gives a single cell in the meridional circulation. The structures of u_s (solid) and ϕ_s (dash-dotted) have maxima over the Northern Hemisphere [when using (4.2a) (cf. Fig.

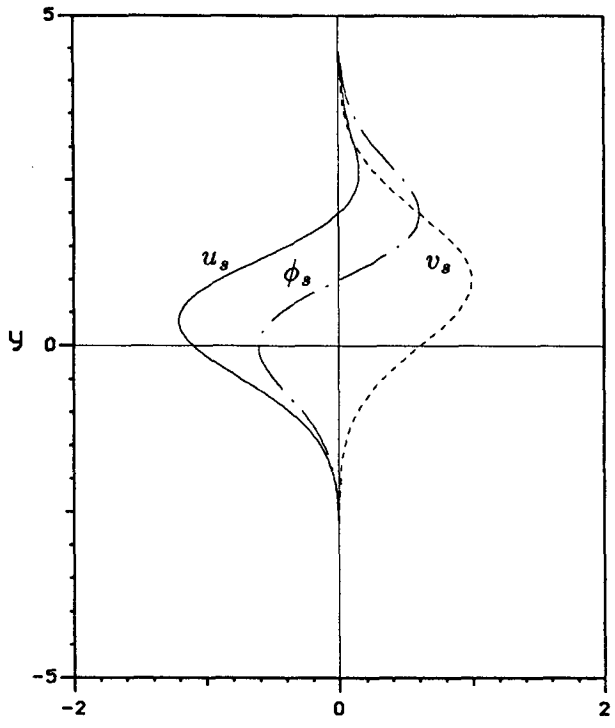

FIG. 2. The meridional profile of the variables u_s (solid), v_s (dotted), and ϕ_s (dash-dotted).

2) or over the Southern Hemisphere when using (4.2b)—not shown].

The time dependence of the first-order solution is given by the three unknown functions U_m, U_s, and V_s, for which there are only the two equations (4.10) and (4.13b). We need therefore one more equation; that is, the second-order balance must be taken into account. The easiest way to do so is to use (2.8), yielding

$$Lv_s^{(2)} = \frac{\partial^2 V_s}{\partial T^2} H_{vs}(y) + 2RV_sH_{vs}(y) + R^2V_sH_{vs}(y) - 2\xi_0^{(1)}yV_sH_{vs}(y) - \nu\left(\frac{\beta}{\beta_a}\right)^{1/2} V_sU_myH_{vs}\frac{\partial H_{um}}{\partial y} \equiv F. \quad (4.14)$$

The solvability condition of (4.14) is

$$\langle F, H_{vs}\rangle = 0, \quad (4.15)$$

where the inner product is given by

$$\langle A, B\rangle \equiv \int_{-\infty}^{\infty} A(y)B(y)dy. \quad (4.16)$$

With (4.14), one obtains

$$\frac{\partial^2 V_s}{\partial T^2} - (2\xi_0^{(1)}\xi_{0c} - R^2)V_s + 2R\frac{\partial V_s}{\partial T} + \nu\alpha V_sU_m = 0, \quad (4.17)$$

where

$$\alpha = -\frac{(\beta/\beta_a)^{1/2}\langle yH_{vs}\partial H_{um}/\partial y, H_{vs}\rangle}{\|H_{vs}\|^2} = \frac{1}{4\sqrt{2}}, \quad (4.18a)$$

$$\|H_{vs}\|^2 = \langle H_{vs}, H_{vs}\rangle. \quad (4.18b)$$

This completes the closed system for determining the first-order solution

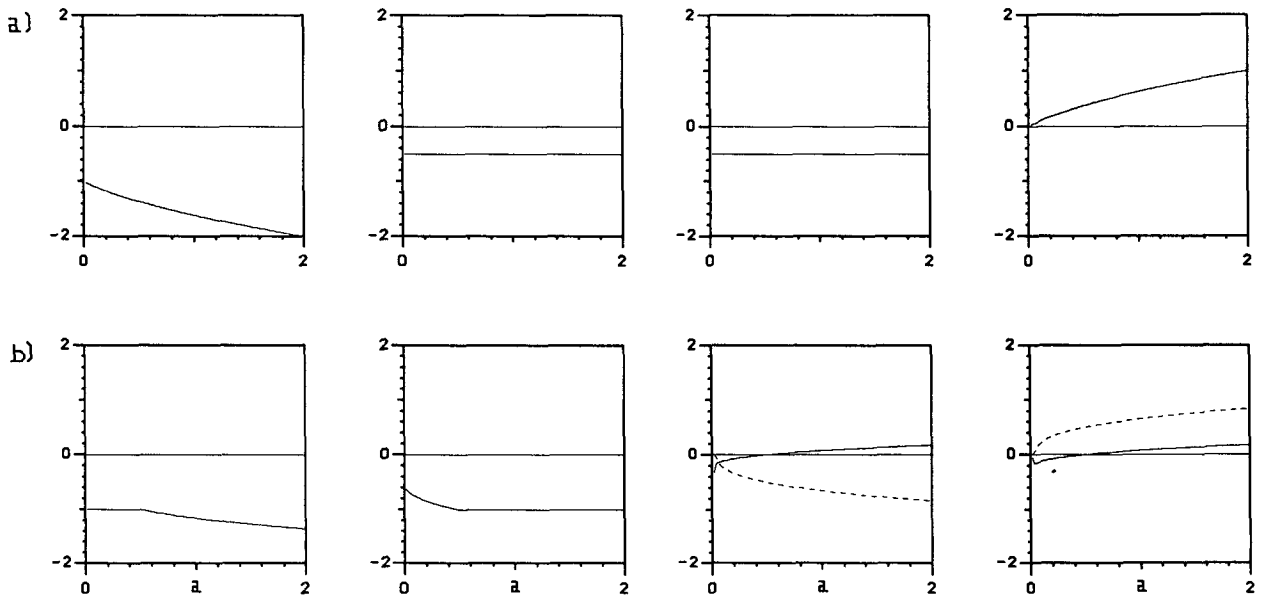

FIG. 3. Eigenvalues of system (5.5, 5.6) as a function of the parameter a for $R = 0.5$. (a) For equilibrium P_0; (b) for equilibria P_1 and P_2. λ_r is shown solid, λ_i is dashed.

$$\frac{\partial^2 V_s}{\partial T^2} + 2R\frac{\partial V_s}{\partial T} - aV_s + \nu\alpha V_s U_m = 0, \quad (4.19a)$$

$$\frac{\partial U_s}{\partial T} + RU_s - V_s = 0, \quad (4.19b)$$

$$\frac{\partial U_m}{\partial T} + RU_m - \nu U_s V_s = 0, \quad (4.19c)$$

where

$$a = 2\xi_0^{(1)}\xi_{0c} - R^2. \quad (4.20)$$

The system (4.19) has a solution in the form of Jacobi elliptic functions. Neglecting the nonlinear terms and friction, this system reduces to the linear, inviscid case discussed in section 3. When $a > 0$, the reduced linear system is unstable. However, the nonlinearity in the full system (4.19) will suppress, as we shall see in the next section, the linear growth rate and lead to finite amplitudes. Equations (4.19) are quite close to those obtained by Pedlosky and Frenzen (1980) in their weakly nonlinear analysis of the midlatitude baroclinic instability problem. The study of the solution of system (4.19) is the topic of the next section.

5. Oscillatory solutions

a. *Stability analysis*

Introducing new dependent variables

$$X = \alpha\nu U_m, \quad Y = \alpha^{1/2}\nu U_s,$$

$$Z = \alpha^{1/2}\nu V_s, \quad W = \frac{\partial Z}{\partial T}, \quad (5.1)$$

system (4.19) becomes

$$\dot{X} = -RX + YZ, \quad (5.2a)$$

$$\dot{Y} = -RY + Z, \quad (5.2b)$$

$$\dot{Z} = W, \quad (5.2c)$$

$$\dot{W} = aZ - 2RW - XZ. \quad (5.2d)$$

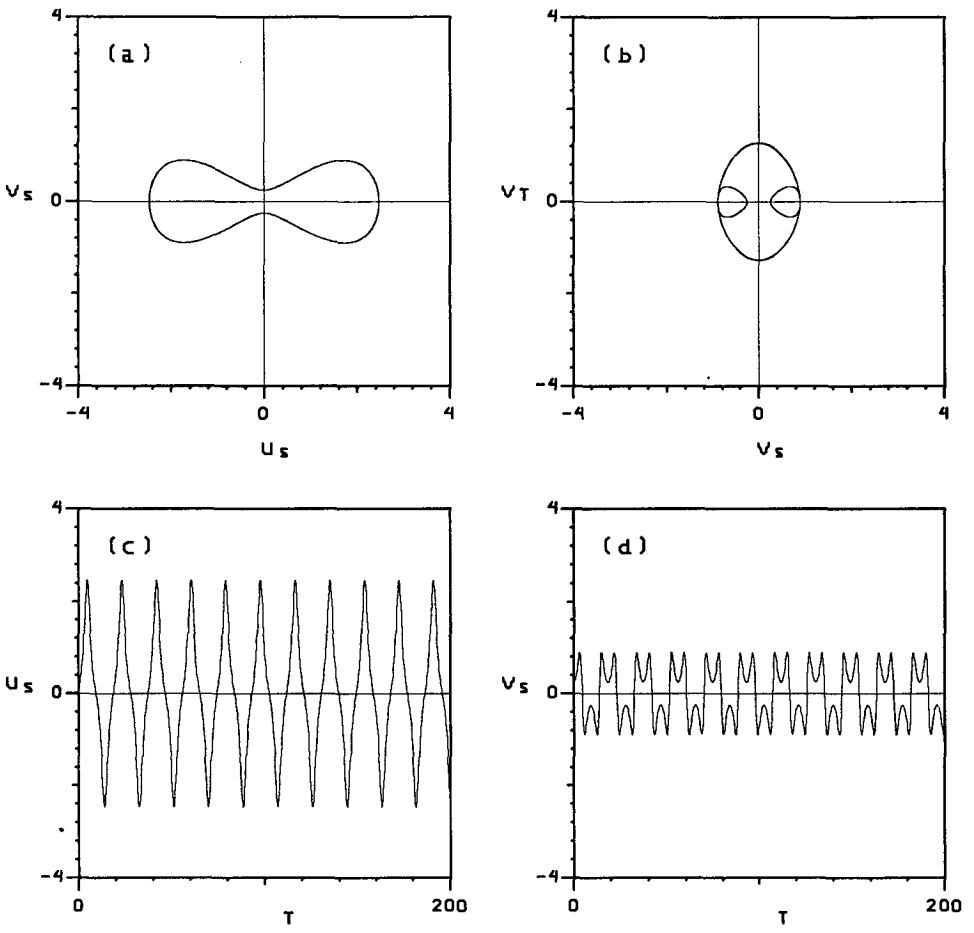

FIG. 4. Inviscid solutions ($R = 0$) of Eq. (5.9) for the case $a = 0.5$, $Z_0 = 0.2$. Trajectories in the (U_s, V_s) and $(V_s, \partial V_s/\partial T)$ plane are shown in (a) and (b), respectively; the time variations of components U_s and V_s are shown in (c) and (d).

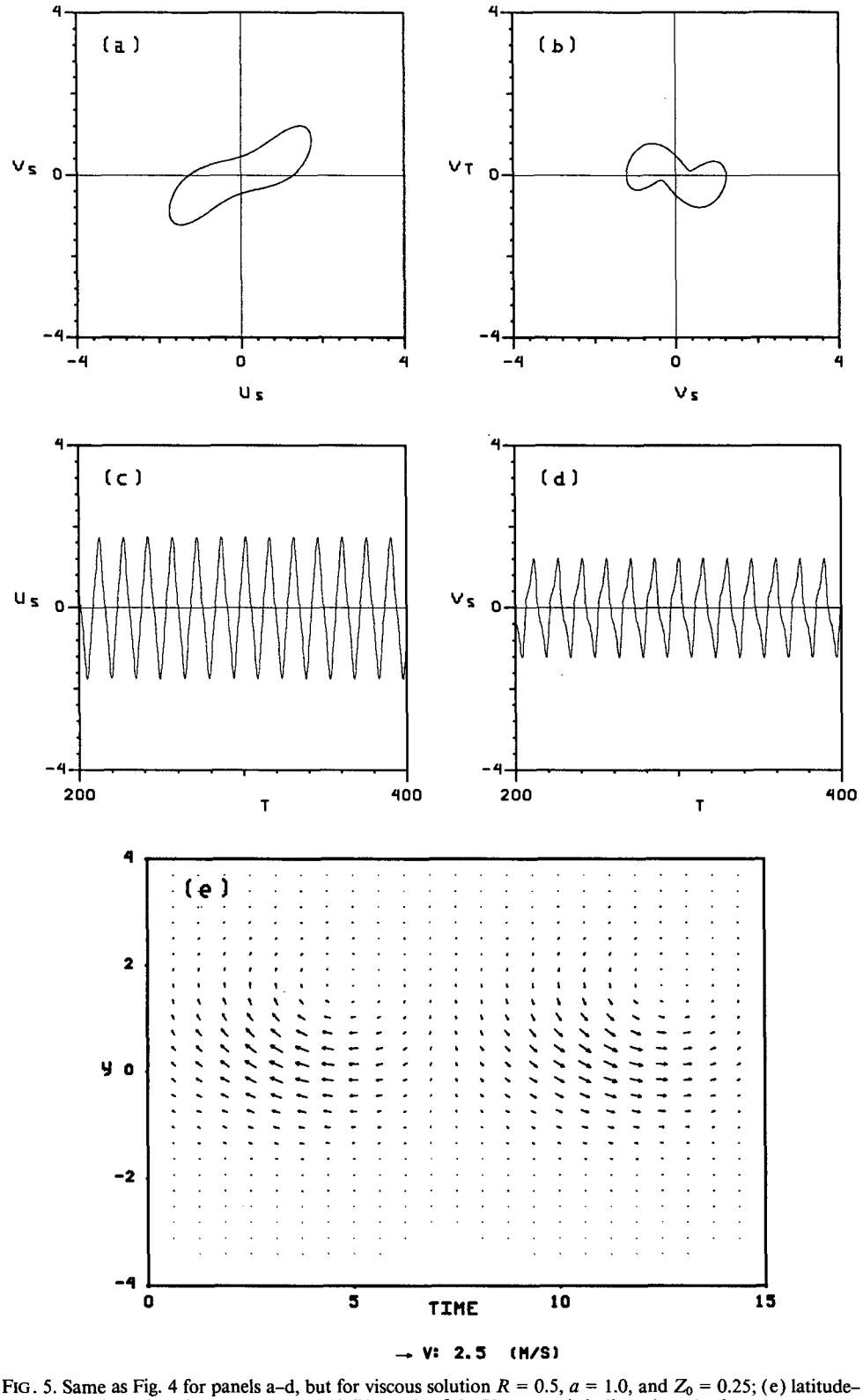

FIG. 5. Same as Fig. 4 for panels a–d, but for viscous solution $R = 0.5$, $a = 1.0$, and $Z_0 = 0.25$; (e) latitude–time plot of $\mathbf{V}_s$ over one period. The scale of the $\mathbf{V}_s$ vectors is indicated on the figure.

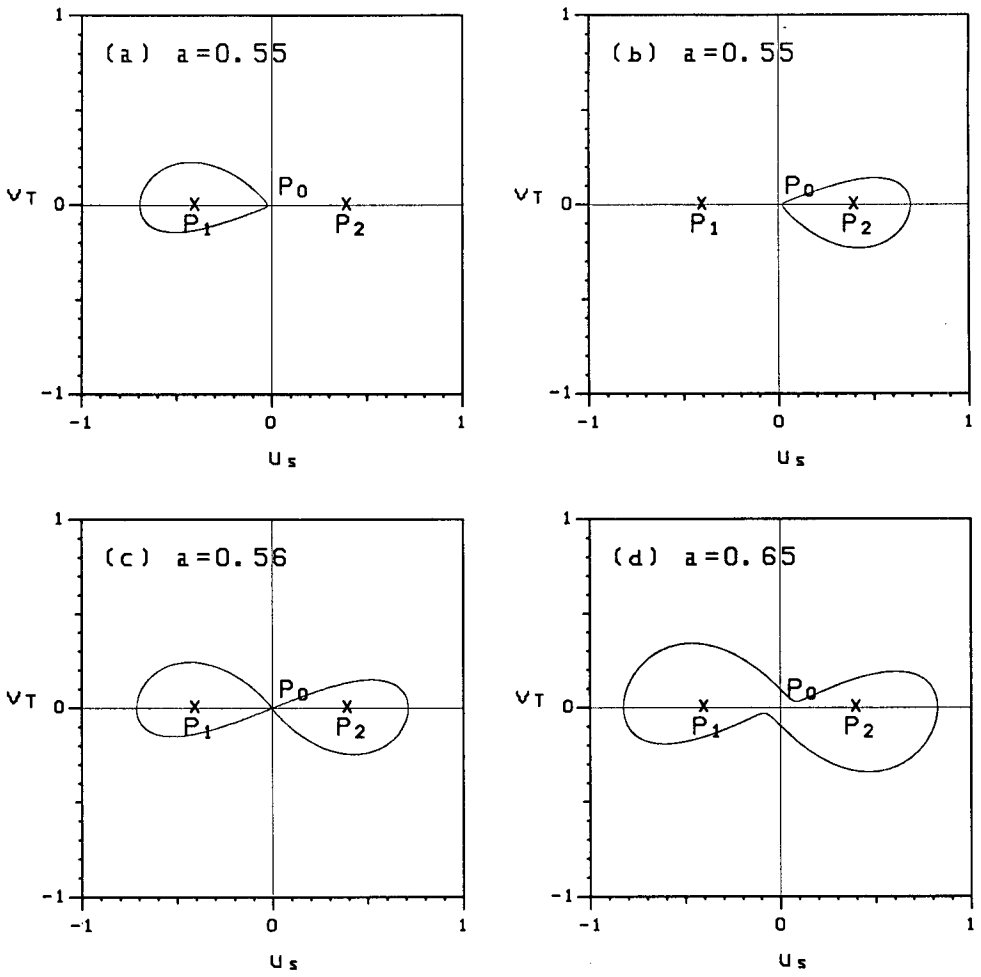

FIG. 6. Numerical solutions of system (4.19) for different parameter values a; $R = 0.5$. Panels (a–d) show the limit cycle projected onto the $(U_s, \partial V_s/\partial T)$ plane; (e–h) show the time variation of U_s.

Three stationary solutions of (5.2) are easily obtained; with $P \equiv (X, Y, Z, W)$, they are

$$P_0 = (0, 0, 0, 0), \quad P_{1,2} = (a, \pm\sqrt{a}, \pm R\sqrt{a}, 0). \tag{5.3a,b,c}$$

Therefore, we have a "pitchfork" bifurcation at $a = 0$. When $a < 0$, the system is inertially stable and all perturbations will die. When $a > 0$, the basic state becomes unstable and two additional equilibria appear (e.g., Guckenheimer and Holmes 1983, §3.4; Ghil and Childress 1987, p. 111). They represent two different meridional cells with opposite circulations, because u_s and v_s have different sign in the equilibria. However, the nonlinear correction through momentum transport is the same so that u_m is the same in the two equilibria. This correction modifies the unstable basic flow and stops its linear instability [cf. Eq. (4.19a)] so as to achieve the equilibrium.

In order to study the stability of these steady-state solutions, we linearize Eqs. (5.2) by

$$P' = P - P_i, \quad i = 0, 1, 2, \tag{5.4}$$

to yield

$$\dot{P}' = L_i P', \quad i = 0, 1, 2, \tag{5.5}$$

where

$$L_i = \begin{pmatrix} -R & Z_i & Y_i & 0 \\ 0 & -R & 1 & 0 \\ 0 & 0 & 0 & 1 \\ -Z_i & 0 & a - X_i & -2R \end{pmatrix}. \tag{5.6}$$

The characteristic equation of (5.6) is

$$\begin{vmatrix} \lambda + R & -Z_i & -Y_i & 0 \\ 0 & \lambda + R & -1 & 0 \\ 0 & 0 & \lambda & -1 \\ Z_i & 0 & -(a - X_i) & \lambda + 2R \end{vmatrix} = 0. \tag{5.7}$$

The four eigenvalues $\lambda = \lambda_r + i\lambda_i$ are shown in Fig. 3, as a function of the supercriticality parameter a.

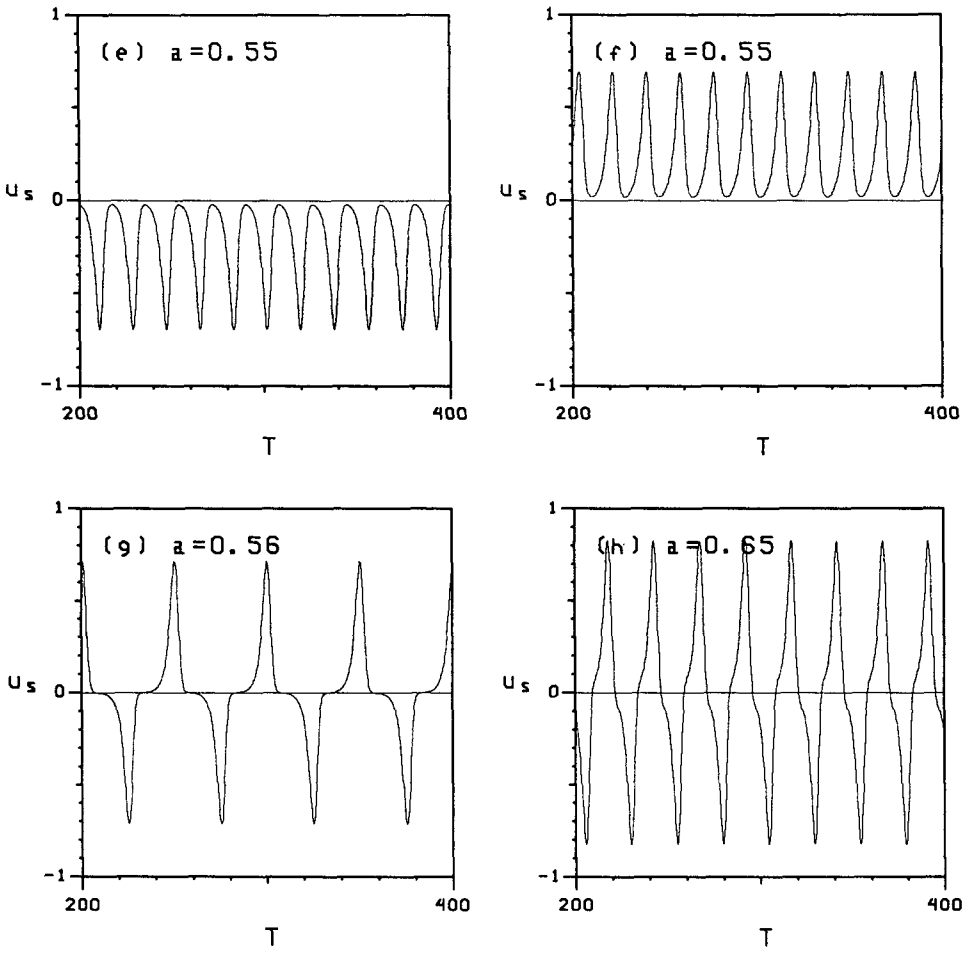

FIG. 6. (*Continued*)

The equilibrium P_0 is always unstable for positive a; that is, one of its eigenvalues is $\lambda > 0$. All eigenvalues in this case are real, in agreement with the analysis of section 3. For the other two equilibria, P_1 and P_2, λ_r changes from negative to positive at a critical value of a; for example, $a_c = 0.5$ for the case $R = 0.5$. This occurs for a complex conjugate pair of eigenvalues, that is, a_c is a Hopf bifurcation point (e.g., Ghil and Childress 1987, §12.2); at the same value of a_c, both equilibria lose their stability and bifurcate each into a limit cycle. The details of the bifurcation sequence will be discussed below.

b. Inviscid solutions

For simplicity, we consider the inviscid case first. Setting $R = 0$ and assuming

$$X(0) = Y(0) = W(0) = 0, \quad Z(0) = Z_0, \quad (5.8)$$

the system reduces to a very simple, first-order equation:

$$\dot{Y}^2 - aY + \frac{1}{12} Y^4 - Z_0^2 = 0. \quad (5.9)$$

This equation is similar to that obtained by Pedlosky and Frenzen (1980) for an inviscid midlatitude problem. Equation (5.9) can be rewritten as

$$\dot{Y}^2 = \frac{1}{24}(d_1^2 - Y^2)(d_2^2 + Y^2)$$

or as

$$\dot{Y} = \frac{1}{24}\sqrt{(d_1^2 - Y^2)(d_2^2 + Y^2)}, \quad (5.10)$$

where

$$d_1^2 = \frac{1}{24}(a + \sqrt{a^2 + Z_0^2/3}),$$

$$d_2^2 = \frac{2Z_0^2}{(a + \sqrt{a^2 + Z_0^2/3})}. \quad (5.11a,b)$$

The solution is given by a Jacobi elliptic function of the first kind with the period

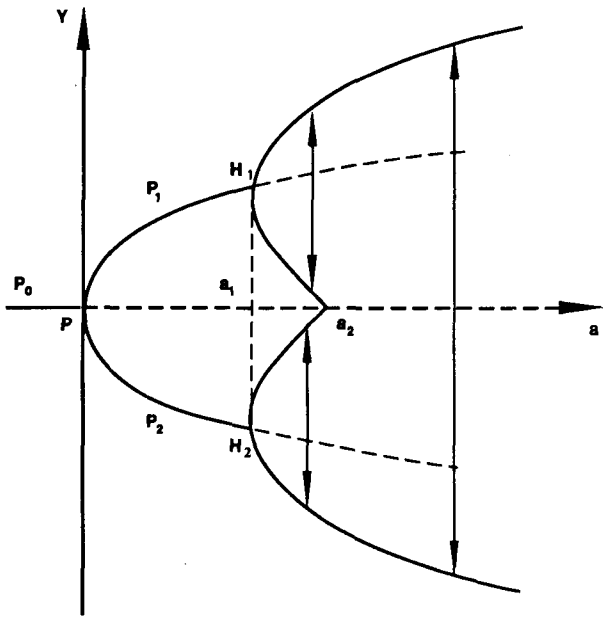

FIG. 7. Bifurcation tree for the system (4.19): point P indicates a pitchfork bifurcation, H_1 and H_2 indicate Hopf bifurcations.

$$T_0 = \frac{1}{\sqrt{24(d_1^2 + d_2^2)}} F\left(\frac{d_1}{\sqrt{d_1^2 + d_2^2}}, \frac{\pi}{2}\right), \quad (5.12)$$

F being the elliptic function. From (5.11), (5.12) it is clear that the period of the system depends on the parameter a and initial value Z_0. The dependence of period on initial value appears only, as expected, in the inviscid system. We discuss the more relevant unique periodicity for viscous solutions in the next subsection.

Figure 4 gives the numerical solution of Eq. (5.9), with the nondimensional parameter values of $a = 0.5$ and $Z_0 = 0.2$. It is found that the amplitudes of the vertical shear in the zonal and meridional wind fields do exhibit regular oscillations with a nondimensional period of $T_0 = 18$. The period in dimensional units is given, according to Eqs. (2.6c) and (4.4g), by

$$t_0 = \epsilon^{1/2} \tau T_0. \quad (5.13)$$

Substituting $\epsilon^{1/2} = 0.4 \sim 0.5$, to yield $\xi_0 \approx 1.25$ in (4.4a) with $\xi_0^{(1)} = O(1)$, and $\tau = \frac{2}{3}$ day from Table 1, gives a dimensional period of $t_0 = 24$–30 days.

c. *Limit cycle in the presence of friction*

In the viscous case, Fig. 5 gives the numerical solution of system (4.19) with parameter values $R = 0.5$, $a = 1.0$, and $Z_0 = 0.25$. The figure clearly shows a finite-amplitude oscillation. By contrast with the inviscid solution, the dependence on the initial value disappears when damping processes are considered. All solutions tend, within a short time, to a limit cycle with a period of about $T_0 = 16$. By equation (5.13) and the choice of ϵ and τ from Table 1, this yields a dimensional period of $t_0 = 21$–26 days.

The time–latitude plot of V_s over one complete period is shown in Fig. 5e. This plot is produced by using the time-dependent amplitude shown in Fig. 5a and the horizontal structure in Fig. 2. The interesting feature of the plot is that the momentum transport associated with the solution changes sign during the oscillation. The strong negative correlation between u_s and v_s destroys momentum balance in the equilibrium states and results in oscillatory solutions. In the equilibrium states, the wind-shear vector at a given latitude (not shown) is either pointing northeast (at the upper level) or southwest. However, in the oscillatory solution, the vector changes from northwest to southeast, and as a result the Coriolis force of the meridional circulation is not in instantaneous balance with zonal friction. This physical mechanism leading to oscillation appears to be worth investigating with observational data.

Numerical solutions for other parameter values are shown in Fig. 6. When $0 < a < a_c \approx 0.5$ (not shown), there are two distinct stable equilibria, each with its own basin of attraction. At $a = a_c$, the two equilibria lose their stability. A limit cycle, with small amplitude at first, appears around each of the previous equilibria (Figs. 6a,b). The two limit cycles increase in size as the parameter a increases. At last they merge into one large limit cycle (Figs. 6c,d) with about twice the period and with peaks of opposite signs in the zonal components (Figs. 6g,h).

The period of the limit cycle depends most strongly on the supercritical wind shear, which is measured by the parameter a [cf. Eqs. (4.19a), (4.20)]. At first, when a increases, the period also increases. In the merged case both period and amplitude are doubled. Afterwards, the amplitude increases while the period decreases and becomes close to the original one. It follows that the periodicity of these nonlinear, viscous oscillations is quite robust and close to 20–30 days in a large-parameter domain.

Information on this system can be summarized in terms of a bifurcation tree as shown in Fig. 7, in which Y represents one component of the solution and a is the supercritical wind shear. When a is negative, the system is inertially stable, and any perturbation will die out. When a becomes positive, the basic state becomes unstable, giving rise to a pitchfork bifurcation, which leads to multiple equilibria. Among the three possible equilibria, the middle one is inertially unstable; the other two are stable.

When a increases further and reaches a_1, these two equilibria also become unstable. At this point, we have two Hopf bifurcations, which give rise each to a periodic solution. As a grows further, the amplitudes of these two periodic solutions become larger and larger, and at a_2, they eventually merge into one periodic so-

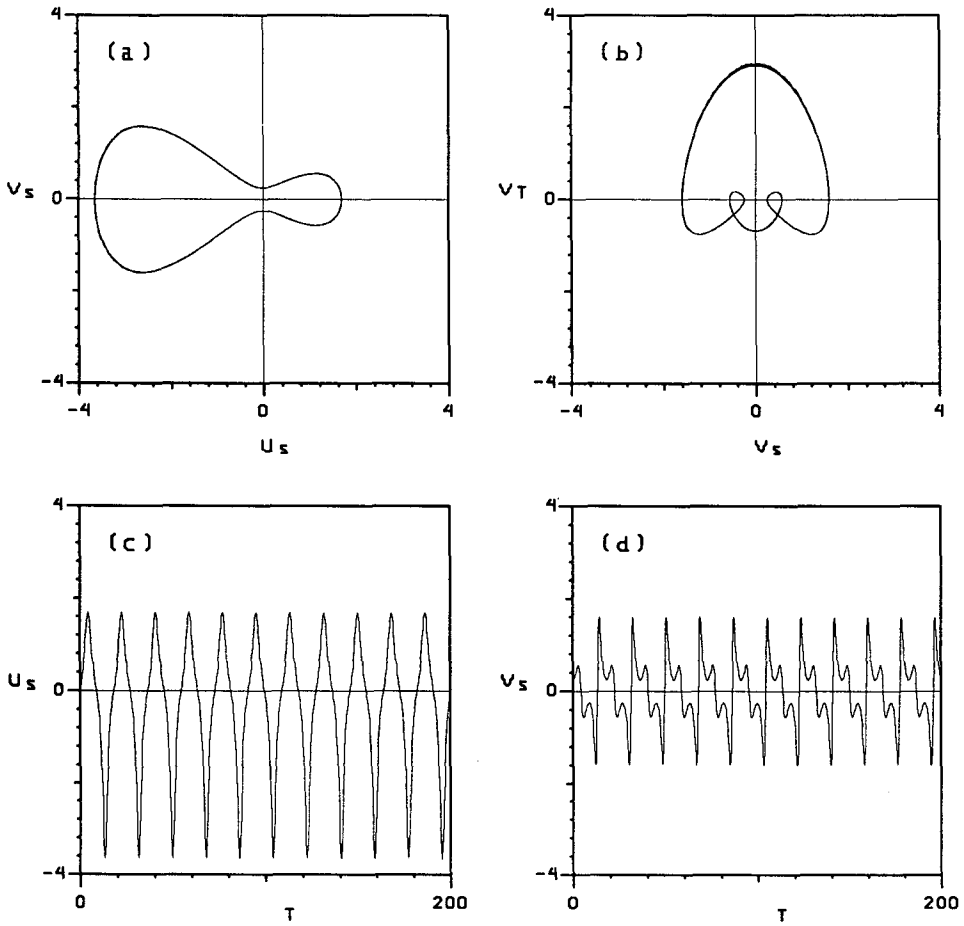

FIG. 8. Same as Fig. 4, but with vertical shear, $b = 0.25$.

lution; afterwards, there is only one periodic solution, as shown in Figs. 6c,d.

6. Solutions with vertical shear

Starting again from Eq. (2.7), we now consider a weak vertical shear of the basic flow, $\zeta \neq 0$, which was neglected in sections 3–5, with the scaling

$$\zeta = \epsilon^{1/2}\zeta^*. \tag{6.1}$$

The first-order equations in a weakly nonlinear expansion (4.4) are

$$\dot{X} = -RX + YZ, \tag{6.2a}$$

$$\dot{Y} = -RY + Z, \tag{6.2b}$$

$$\dot{Z} = W, \tag{6.2c}$$

$$\dot{W} = aZ - 2RW - XZ - bYZ, \tag{6.2d}$$

where

$$b = -\frac{\zeta^*}{\alpha}\left(\frac{\beta}{\beta_a}\right)^{1/2}\left\langle yH_{vs}\frac{\partial^3 H_{vs}}{\partial y^3}, H_{vs}\right\rangle \Big/ \|H_{vs}\|. \tag{6.3}$$

Considering the vertical wind shear introduces the new parameter b of Eqs. (6.2d, 6.3). The second nonlinear term of Eq. (6.2d) is the only difference from the previous system (5.2): it is the only term that arises from the vertical shear in the basic flow. Numerical solutions of Eqs. (6.2) without and with friction are shown in Figs. 8 and 9, respectively. Comparing these with Figs. 4 and 5, it is apparent that the period of the oscillations is almost the same, but the symmetry $(X, Y, Z, W) = (X, -Y, -Z, -W)$ of the inviscid solutions is lost. Figure 9e shows the same basic northwest–southeast oscillation of the wind-shear vector $\mathbf{V}_s$ as in Fig. 5e (where $\zeta = 0 = b$).

The bifurcation tree, shown in Fig. 10, is also more complicated than in the previous case of $\zeta = 0$. The basic state now becomes unstable at a_{-1}, which is below

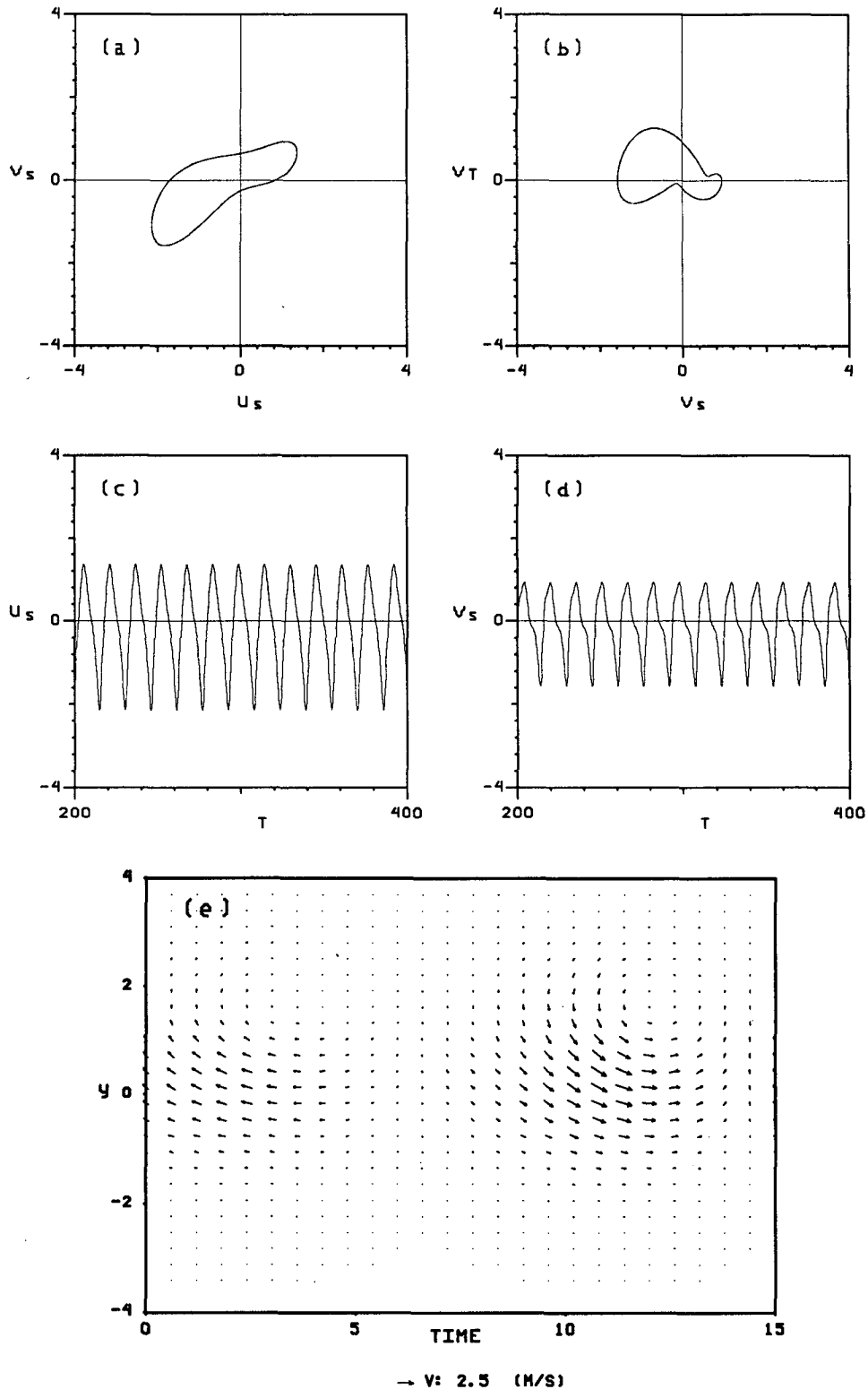

FIG. 9. Same as Fig. 5, but with vertical shear, $b = 0.25$.

zero. This is because the vertical shear contributes kinetic energy to make the state unstable. Furthermore, the loss of symmetry transforms the pitchfork bifurcation occurring at $a = 0$ in Fig. 7 into a transverse bifurcation (e.g., Guckenheimer and Holmes 1983, §3.4). As a result, for $a_{-1} < a < a_1$, there exist two stable branches and one unstable branch of steady solutions. The lower branch P_2 loses its stability at a_1 through Hopf bifurcation. Thus, a stable periodic solution around the lower branch coexists with the stable steady solution of the upper branch P_1.

Once the periodic solution arising at H_2 increases in amplitude so as to touch the unstable branch of steady solutions P_0 in the middle, this periodic solution itself disappears in a so-called global bifurcation (Guckenheimer and Holmes 1983, Chapter 6). Hence, between a_2 and a_3, only one stable solution exists. This steady solution becomes unstable in turn and gives rise to a new periodic solution through Hopf bifurcation at a_3. When this periodic solution touches the unstable branch P_0 in the middle, the two periodic solutions merge into one large attractor set.

It is interesting to follow the change in the solutions of system (6.2) and in their stability as the parameter a increases. The numerical solutions of system (6.2) for different values of the parameter a are shown in Fig. 11. For $R = 0.5$, $b = 0.25$, the point $a = 0.2$ lies in the interval (a_{-1}, a_1), and there are two stable equilibria, P_1 and P_2 (not shown). For $a_1 < a = 0.43 < a_2$, P_1 is still a stable solution, while P_2 has lost its stability to a limit cycle (Fig. 11a). Here P_1 becomes unstable at a_2 and the trajectory leaves its neighborhood and goes to the stable steady solution P_2 (Fig. 11b). For $a_2 < a < a_3$ trajectories tend to the limit cycle around P_2. In Fig. 11c, $a_3 < a < a_4$ and the two trajectories starting near P_1 (solid) and near P_2 (dashed) tend both to the same limit cycle.

When $a > a_4$ (Fig. 11d), the behavior of the oscillations changes again: solutions starting near either P_1 or P_2 describe irregular loops around both unstable branches. Such behavior is reminiscent of the loops described by the trajectories in the classical Lorenz (1963) system around the two unstable convective states. This similarity is confirmed by considering, in Figs. 11e–h, the time variations of the zonal component u_s corresponding to Figs. 11a–d, respectively. It is clear from Fig. 11h that the number of loops with positive and with negative zonal wind is irregularly distributed, and does not depend on whether the initial wind is easterly or westerly. The transition to and detailed description of this aperiodic behavior are beyond the purpose of the present work.

The robustness of the period persists in the presence of vertical shear. In Figs. 11a,c the period is very similar to those we found in sections 4 and 5. In the case of Figs. 11d,h, there are two basic periods, one of which is much longer. But the principal one, which corresponds to the smaller-amplitude oscillation, is still close to the previous ones. This robustness of the nonlinear SII oscillation gives us some confidence in relating it to low-frequency oscillations observed in the tropical atmosphere.

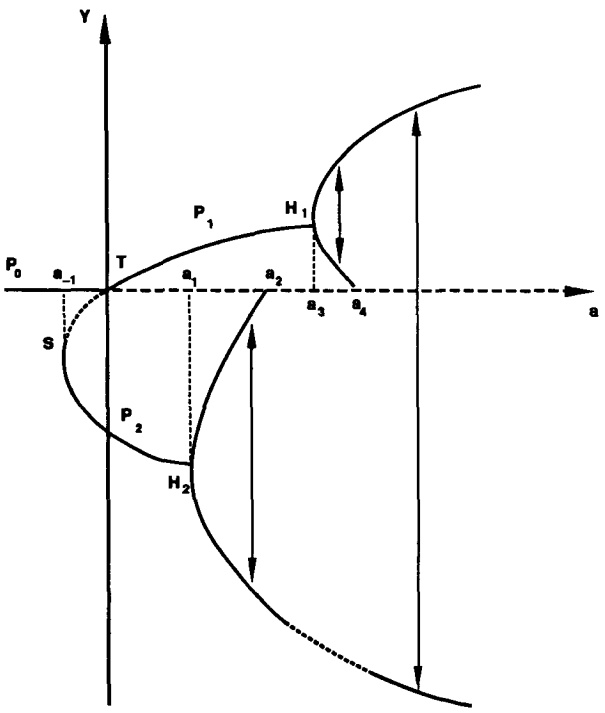

FIG. 10. Same as Fig. 7, but with vertical shear, $b = 0.25$: T is a transverse and S a saddle-node bifurcation, H_1 and H_2 being Hopf bifurcations.

7. Conclusions

The linear and nonlinear characteristics of the symmetric inertial instability (SII) that develops in a horizontally sheared basic flow on an equatorial β plane have been studied in a simple two-layer symmetric model. Our weakly nonlinear analysis extends the linear theory of Dunkerton (1981) and Stevens (1983).

Both constant shear and curvature of the basic-flow wind profile are important in producing SII: the curvature reduces the stabilizing β effect and therewith the critical value of constant shear. It is found that a smaller static stability, and hence a smaller equivalent Rossby radius, also favor the establishment of SII. The most unstable mode is a baroclinic mode with a single cell in the meridional direction, as found by Stevens (1983). The zonal flow components are in quasigeostrophic balance, and the meridional component is much smaller than the zonal one. A weak barotropic mode is nonlinearly initiated by momentum transport. In the inviscid case, solutions can be found in terms of Jacobi elliptic functions. In this case, periodic solutions exist for each initial state, which determines the

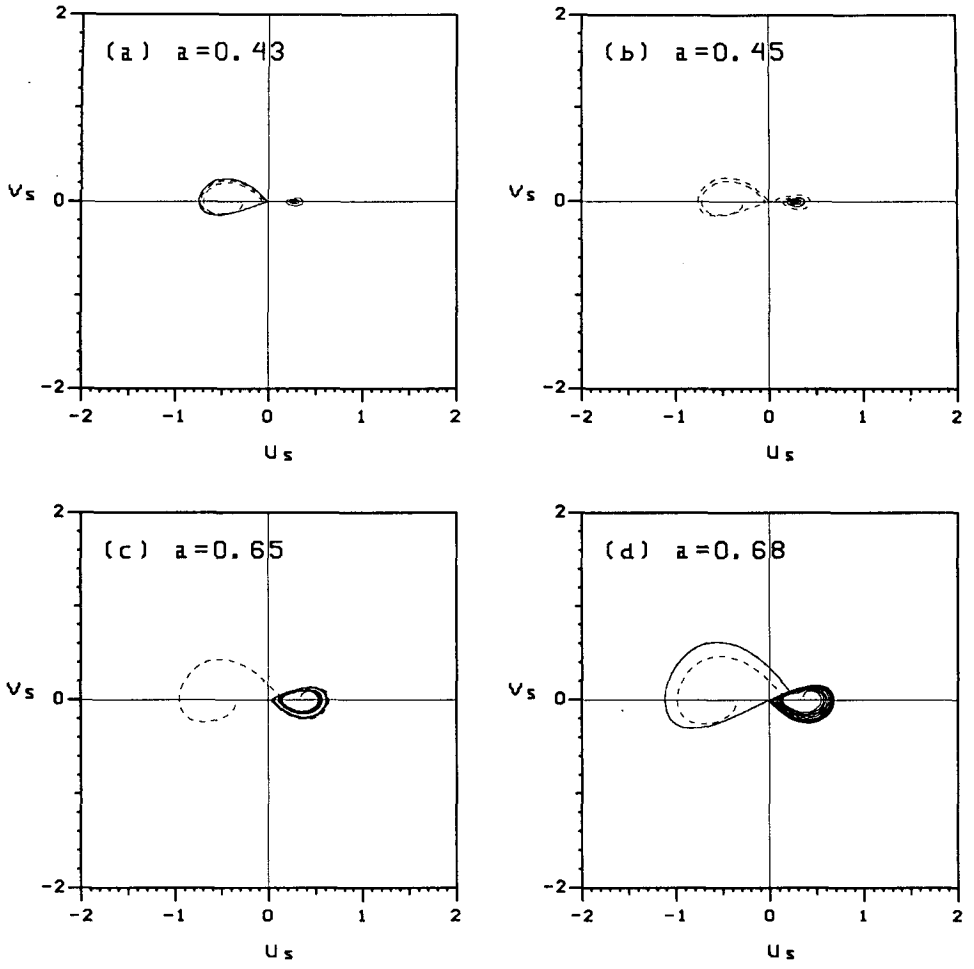

FIG. 11. Same as Fig. 6, but with vertical shear, $b = 0.25$. Two trajectories are shown in each panel: one starts near the lower branch (dashed), the other near the upper branch (solid).

corresponding amplitude and period; they are neutrally stable to perturbations.

Thermal and mechanical dissipation processes select a finite number, one or two, of periodic solutions, each of which is asymptotically stable, that is, a limit cycle. The period of each limit cycle is basically determined by the supercritical shear, but this dependence is weak for a large and physically reasonable parameter range. The exact value of this nearly constant period cannot be determined in the present weakly nonlinear approach, but for the evidently plausible choices made in Table 1, it is of about 20–30 days.

As mentioned in section 1, Anderson and Rosen (1983), Krishnamurti and colleagues (1982, 1988), and Stevens (1983) all suggested a connection between SII and the 40–50-day oscillation of Madden and Julian (1971, 1972). But the 40–50-day oscillation has two important features not easily explained by SII: one is its obviously nonsymmetric and zonally propagating character, with a wavenumber-one wind anomaly traveling eastward; the other is the crucial role of latent heat release over the Maritime Continent. In contradistinction, Ghil and Mo (1991) detected a 24–28-day oscillation that has uniform strength throughout the tropics, while the 40–50-day oscillation is mostly confined to the Indian Ocean and the western Pacific. It appears, therefore, that nonlinear SII, with its plausible period of 20–30 days, is a more likely explanation for the 24–28-day oscillation than for the 40–50-day one.

The physical mechanism of the stable viscous oscillations in our model is related to instantaneous imbalances between the Coriolis force associated with the meridional circulation and the zonal friction force. The anomaly flow patterns, as shown in Fig. 5e and Fig. 9e, are much more pronounced over the Northern Hemisphere where the basic flow is westerly. The zonal flow fluctuations do not change the direction of the total flow, but the meridional component leads to fluctuations of divergence and convergence in the wind field. These oscillations in the divergence of flow might have an impact on the intensity of monsoon rainfall and the severity of monsoon breaks (Sikka and Gadgil

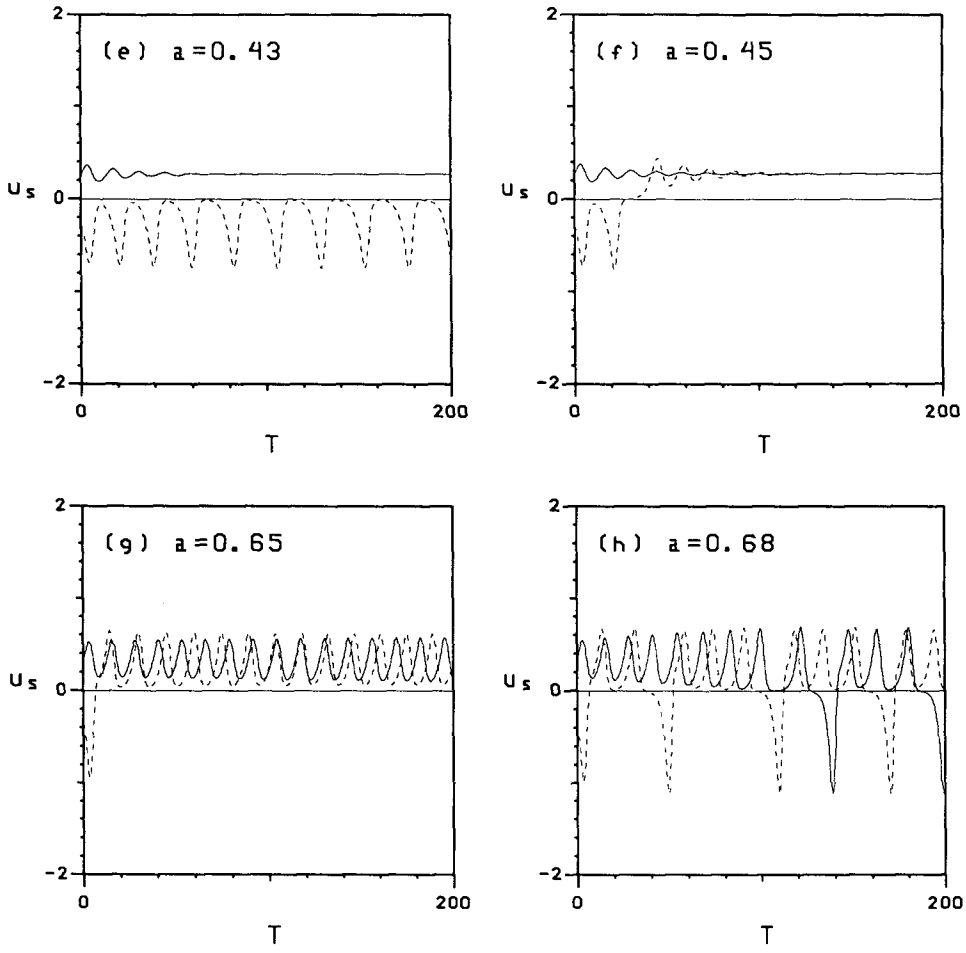

FIG. 11. (*Continued*)

1980). Such 20–30-day oscillations in the zonally symmetric component of tropical divergence could be studied in the data and, if found, be related to the Indian and West African monsoons.

We also studied a basic flow with a constant, weak vertical shear. Both inviscid and viscous solutions lose their symmetry in the presence of this vertical shear. The properties of the periodic solutions are otherwise quite similar to those without vertical shear. But aperiodic solutions with an irregular number of easterly and westerly wind episodes also arise in this case.

The oscillatory behavior in the symmetric component of the tropical circulation is much more complex than what can be accounted for by such a simple model. Many additional physical processes, as pointed out by Webster and Chou (1983), Goswami and Shukla (1984), and others, could be important. In addition to the present dynamic instability, thermodynamical and moist processes as well as their nonlinear interaction with the dry dynamics could help us get a better understanding of this complex problem.

To conclude, it might be worthwhile to point out that the detailed dynamics and physics of other fluid dynamical and meteorological phenomena to which SII ideas have been applied might be quite different. Hence our analysis, e.g., the exact scaling relations, will not be directly applicable to the tropical stratosphere (Dunkerton 1981), midlatitude cyclones (Solberg 1936), or mesoscale disturbances (Emanuel 1979; Xu 1986; Thorpe and Rotunno 1989). But the bifurcation trees of Fig. 7 with mirror symmetry, or Fig. 10 without it, are fairly common and structurally stable, that is, independent of small changes in the parameters or even in the governing equations (Guckenheimer and Holmes 1983; Ghil and Childress 1987). Hence, it is likely that finite-amplitude oscillations could be found in other applications of SII, upon careful and systematic consideration of nonlinearities.

Acknowledgments. It is a pleasure to thank A. Arakawa, F.-F. Jin, J. D. Neelin, S. V. Venkateswaran, and M. Yanai for helpful comments on an earlier version of the typescript or for useful suggestions. Q. Xu and an anonymous referee made pertinent comments

and helped improve the presentation. This work was supported by NSF Grants ATM86-15424 and ATM90-13217 and by NASA Grant NAG-5713.

REFERENCES

Anderson, J. R., and R. D. Rosen, 1983: The latitude-height structure of 40–50 day variations in atmospheric angular momentum. *J. Atmos. Sci.*, **40,** 1584–1591.

——, and D. E. Stevens, 1987: The presence of linear wavelike modes in a zonally symmetric model of the tropical atmosphere. *J. Atmos. Sci.*, **44,** 2115–2127.

Boyd, J. P., 1978a: The effects of latitudinal shear on equatorial waves. Part I: Theory and methods. *J. Atmos. Sci.*, **35,** 2236–2258.

——, 1978b: The effects of latitudinal shear on equatorial waves. Part II: Applications to the atmosphere. *J. Atmos. Sci.*, **35,** 2259–2267.

——, and Z. D. Christidis, 1982: Low wavenumber instability on the equatorial beta-plane. *Geophys. Res. Lett.*, **9,** 769–772.

Dunkerton, T. J., 1981: On the inertial stability of the equatorial middle atmosphere. *J. Atmos. Sci.*, **38,** 2354–2364.

——, 1982: The double-diffusive modes of symmetric instability on an equatorial beta-plane. *J. Atmos. Sci.*, **39,** 1653–1657.

——, 1983: A nonsymmetric equatorial inertial instability. *J. Atmos. Sci.*, **40,** 807–813.

Emanuel, K. A., 1979: Inertial instability and mesoscale convective systems. Part I: Linear theory of inertial instability in rotating viscous fluids. *J. Atmos. Sci.*, **36,** 2425–2449.

——, 1983: The Lagrangian parcel dynamics of moist symmetric instability. *J. Atmos. Sci.*, **40,** 2368–2376.

Fjørtoft, R., 1944: On the frontogenesis and cyclogenesis in the atmosphere. Part I: On the stability of stationary circular vortex. *Geofys. Publ.*, **16**(5), 28 pp.

——, 1950: Application of integral theorems in deriving criteria of stability for laminar flows and for the baroclinic circular vortex. *Geofys. Publ.*, **17**(6), 52 pp.

Ghil, M., and S. Childress, 1987: *Topics in Geophysical Fluid Dynamics: Atmospheric Dynamics, Dynamo Theory, and Climate Dynamics.* Springer-Verlag, 485 pp.

——, and K. C. Mo, 1991: Intraseasonal oscillation in the global atmosphere. Part I: Northern Hemisphere and tropics. *J. Atmos. Sci.*, **48,** 752–790.

Goswami, B. N., and J. Shukla, 1984: Quasi-periodic oscillation in a symmetric general circulation model. *J. Atmos. Sci.*, **41,** 20–37.

Guckenheimer, J., and P. Holmes, 1983. *Nonlinear Oscillations, Dynamical Systems, and Bifurcations of Vector Fields.* Springer-Verlag, 453 pp.

Helmholtz, H. von, 1888: Über atmosphärische Bewegungen. *Meteor. Z.*, **5,** 329–340.

Hunt, B. G., 1981: The maintenance of the zonal mean state of the upper-atmosphere as represented in a three-dimensional general circulation model extending to 100 km. *J. Atmos. Sci.*, **38,** 2172–2186.

Krishnamurti, T. N., and D. Subrahmanyam, 1982: The 30–50 day mode at 850 mb during MONEX. *J. Atmos. Sci.*, **39,** 2088–2095.

——, D. K. Osterhof and A. V. Mehta, 1988: Air–sea interaction on the time scale of 30 to 50 days. *J. Atmos. Sci.*, **45,** 1304–1322.

Lau, K. M., and H. Lim, 1984: On the dynamics of equatorial forcing of climate teleconnections. *J. Atmos. Sci.*, **41,** 161–176.

Lorenz, E. N., 1963: Deterministic nonperiodic flow. *J. Atmos. Sci.*, **20,** 130–141.

Madden, R. A., and P. R. Julian, 1971: Detection of a 40–50 day oscillation in the zonal wind in the tropical Pacific. *J. Atmos. Sci.*, **28,** 702–708.

——, and ——, 1972: Description of global-scale circulations cells in the tropics with a 40–50 day period. *J. Atmos. Sci.*, **29,** 1109–1123.

Ooyama, K., 1966: On the stability of the baroclinic circular vortex: a sufficient criterion for instability. *J. Atmos. Sci.*, **23,** 43–53.

Pedlosky, J., 1971: Finite-amplitude baroclinic waves with small dissipation. *J. Atmos. Sci.*, **28,** 587–597.

——, 1972: Limit cycles and unstable baroclinic waves. *J. Atmos. Sci.*, **29,** 53–63.

——, and C. Frenzen, 1980: Chaotic and periodic behavior of finite-amplitude baroclinic waves. *J. Atmos. Sci.*, **37,** 1177–1196.

Rayleigh, 1916: On the dynamics of revolving fluids. *Proc. R. Soc. London,* **A93,** 447–453.

Sikka, D. R., and S. Gadgil, 1980: On the maximum cloud zone and the ITCZ over Indian longitudes during the southwest monsoon. *Mon. Wea. Rev.*, **108,** 1840–1850.

Solberg, H., 1936: Le mouvement d'inertie de l'atmosphère stable et son rôle dans la théorie des cyclones. P. V. *Météor.*, U.G.G.I., (Edinburgh), **II,** 66–82.

Stevens, D. E., and R. S. Lindzen, 1978: Tropical wave—CISK with a moisture budget and cumulus friction. *J. Atmos. Sci.*, **35,** 940–960.

——, 1983: On symmetric stability and instability of zonal mean flows near the equator. *J. Atmos. Sci.*, **40,** 882–893.

Thorpe, A. J., and R. Rotunno, 1989: Nonlinear aspects of symmetric instability. *J. Atmos. Sci.*, **46,** 1285–1299.

Webster, P. J., and L. C. Chou, 1981: Low frequency transitions of a simple monsoon system. *J. Atmos. Sci.*, **37,** 368–382.

Xu, Q., 1986: Generalized energetics for linear and nonlinear symmetric instabilities. *J. Atmos. Sci.*, **43,** 972–984.

——, 1988: A formula for eddy viscosity in the presence of moist symmetric instability. *J. Atmos. Sci.*, **45,** 5–8.

——, 1989: Extended Sawyer-Eliassen equation for frontal circulation in the presence of small viscous moist symmetric stability. *J. Atmos. Sci.*, **46,** 2671–2683.

Yanai, M., and T. Tokioka, 1969: Axially symmetric meridional motions in the baroclinic circular vortex: A numerical experiment. *J. Meteor. Soc. Japan,* **47,** 183–198.